International Journal of Engineering & Technology, 7 (4.18) (2018) 84-89

International Journal of Engineering & Technology

Website: www.sciencepubco.com/index.php/IJET

Research paper

Physico-chemical and catalytic properties of Fe-MKSF catalyst: Influence of MKSF clay as catalyst support

Nur Hidayati Abdullah[1], Nor Aida Zubir[1,2,*], Mohammad Khairul Azam Selamat[1], Rasyidah Alrozi[1,2], Norhaslinda Nasuha[1,2], Hawaiah Imam Maarof[3], Benjamin Ballinger[4], Julius Motuzas[5], João C. Diniz da Costa[5]

[1]*Faculty of Chemical Engineering, Universiti Teknologi MARA, Cawangan Pulau Pinang, 13500 Pulau Pinang, Malaysia*
[2]*Hybrid Nanomaterials, Interfaces & Simulation (HYMFAST), Faculty of Chemical Engineering, Universiti Teknologi MARA, Cawangan Pulau Pinang, 13500 Pulau Pinang, Malaysia*
[3]*Faculty of Chemical Engineering, Universiti Teknologi MARA, 40450 Shah Alam, Selangor, Malaysia*
[4]*School of Chemical Engineering, Engineering Campus, Universiti Sains Malaysia, 14300 Nibong Tebal, Penang, Malaysia*
[5]*The University of Queensland, FIM2Lab- Functional Interfacial Materials and Membranes Laboratory, School of Chemical Engineering, Brisbane, Qld 4072, Australia*
**Corresponding author E-mail: noraida709@ppinang.uitm.edu.my*

Abstract

The heterogeneous Fenton-like reaction is one of the most promising and effective treatment methods for the degradation of organic pollutants. In the present study, a detailed investigation on synthesis, characterization, and catalytic activity studies for oxidative degradation of methyl orange (MO) solution by iron oxide-immobilized montmorillonite KSF (Fe-MKSF) and pristine iron oxide catalysts were performed. The catalysts were synthesized via an impregnation-hydrothermal method using an autoclave reactor. Interestingly, the Fe-MKSF showed the highest catalytic removal of MO (85%) compared to the pristine iron oxides (30%) and MKSF (52%). This finding is well supported by the significant increase in surface area of the Fe-MKSF compared to the pristine catalysts (105.8 m^2/g [Fe-MKSF] vs 52.2 m^2/g [iron oxide] and 74.2 m^2/g [MKSF]). The increased in surface area is favorable in having high accessibility of reactants towards the catalysts' active sites which enable to diminish limitations in mass transfer during the reaction. These traits proved to be essential for the improved catalytic activity of the Fe-MKSF catalyst.

Keywords: *Catalytic properties; Fenton-like; Iron oxide; MKSF clay; Nanocomposite.*

1. Introduction

Water pollution is currently one of the major global issues being addressed by the scientists worldwide. A significant part of global water pollution is from dye contaminated wastewater, originating from dye and textile, pharmaceutical and other industries. Dye contaminated wastewater contains a wide variety of recalcitrant organic pollutants [1], which when directly discharged into water bodies, may lead to detrimental effects in both environment and human health due to its toxicity, non-biodegradability and environmental aesthetic impacts [2,3]. It is estimated that more than 700 000 tonnes of dyes are currently being discharged per year, with more than 50% of total discharge attributed to azo dyes [4]. The effluents in dye contaminated wastewater usually contain a high concentration of dyes, nutrients, inorganic salts and hydroxide ions (high pH) [5].

The negative environmental consequences of unmitigated effluent discharge have led to the development of alternative wastewater treatment methods which are efficient, practical and cost effective. Advanced oxidation processes (AOPs) have emerged as a robust and promising method for treating dye contaminated wastewater. AOPs were proven to be effective in degrading various recalcitrant organic pollutants such as aromatic compounds [6, 7], volatile organic compounds [8], as well as inorganic compounds such as sulphides and nitriles [9]. In general, AOPs generate reactive oxygen species (ROS) such as hydroxyl (•OH) radicals and hydroperoxyl (•OOH) radicals that non-selectively degrade the organic pollutants during catalysis.

Among the various AOPs, catalysis using Fenton or Fenton-like reactions seem to be the dominant technology reported in scientific literature. This is likely due to the sufficiency of mild reaction conditions to degrade pollutants; mild reaction conditions utilize lower amounts of energy compared to other AOPs in generating the ROS during catalysis. However, homogeneous Fenton/Fenton-like processes possess some disadvantages compared to rival technologies such as the production of a large quantity of iron sludge which required for secondary treatment, high maintenance costs, efficient performance within a narrow pH range and infeasible catalyst recovery [10]. To avoid these pitfalls, heterogeneous catalysts are used to facilitate Fenton/Fenton-like reactions in place of homogeneous catalysts.

Heterogeneous Fenton-like catalysts have emerged as a promising alternative to homogeneous Fenton catalysts due to their limited drawbacks as well as their high product recovery and long-life span. Various types of iron-containing catalysts have been reported in scientific literature. Such catalysts include bulk containing iron such as hematite (α-Fe_2O_3) [11,12], maghemite (γ-Fe_2O_3) [13], and magnetite (Fe_3O_4) [14,15]. In recently published work, these iron species were immobilized into different types of catalyst supports. The use of a catalyst support enables the deposition and retention of well dispersion of iron species throughout the support structure which increases the catalyst surface area. Currently, numerous types of materials such as clay

[16,17], zeolite [18–20], silica [21,22], graphene oxide [23,24] and other carbon-based materials [25–27] have been used as a catalyst support for heterogeneous Fenton-like catalysts. Amongst these materials, the use of clay catalyst support (i.e. ball clay, montmorillonite K10 and kaolin) has many benefits: [28,29] it is highly abundant, inexpensive, environmentally benign, has a high specific surface area, high chemical and mechanical stability that has unique surfaces and structural properties [30, 31].

Clay has generally been considered a stable catalyst support for Fenton-like reactions due to its ability to sustain catalytic activity over time. Furthermore, the clay material maintains its chemical integrity under operating conditions; minimal leaching of interlayer metal species to the external solution have been detected [32]. There seems to be a clear scientific and experimental link between the immobilization and retention of iron species within the clay support structure and the maintenance of high catalytic activity for heterogeneous catalysis of Fenton-like reactions. However, a detailed investigation of the physico-chemical and catalytic properties of iron species being immobilized onto and/or within the montmorillonite KSF clay has not been reported previously. Hence, the present study shows the detailed investigations on the physico-chemical as well as catalytic properties of resultant composite catalyst once the iron species (i.e., iron oxides) particles being immobilized onto and/or MKSF clay matrix.

2. Experimental

2.1. Synthesis of iron-immobilized montmorillonite KSF clay (Fe-MKSF) composite and iron oxides catalysts

The Fe-MKSF catalyst was synthesized from a reaction solution consisting of iron precursor and dispersion of MKSF clay as described elsewhere [33]. Na_2CO_3 was added slowly to vigorously stirred 0.2M of $FeCl_2.4H_2O$ solution at iron molarity to the MKSF clay of 20 mmol Fe/ g MKSF clay. The solution was continuously stirred for 3 h. Then, MKSF was added into the mixture and stirred for another 3 h. The mixture was then aged at 100°C for 48 h in a Teflon sealed autoclave reactor. The resulting precipitates were centrifugally recovered and washed several times with deionized water and dried at 60°C overnight. The dried samples were calcined in air atmosphere at 350°C for 20 h in a furnace at a ramping rate of 10°C/min. Pristine iron oxides catalyst was synthesized through analogous procedures except for the addition of MKSF clay.

2.2. Characterization

The nitrogen sorption analysis was carried out using Micromeritics ASAP 2020 to investigate the textural and structural properties of the Fe-MKSF, iron oxide and MKSF, respectively. The Brunauer-Emmett-Teller (BET) method was used to determine the surface area of the samples while the Density Functional Theory (DFT) method was used in analyzing the profile of the pore size distribution. Prior to the analysis, the samples were degassed for 24 h at 200°C with a heating rate of 10°C/ min. The samples were further characterized using X-ray diffraction (XRD) analysis (Bruker D8 Advance) for phase determination of crystalline samples. CuKα was used as source of radiation (λ=1.54Å). The diffractometer operated at 40 kV and 40 mA. Thermogravimetric analysis (TGA) was performed on Thermal Advantage Q Series (TA 1000). The uncalcined samples were heated from 30°C to 500°C at a heating rate of 10°C/min using compressed air purged at flow rate of 50 mL/min.

2.3. Catalytic performances

The catalytic performances of the Fe-MKSF catalyst was tested in heterogeneous Fenton-like reaction using methyl orange (MO) as the model pollutant. 0.2 g/L of Fe-MKSF catalyst was added into 35 mg/L of MO solution. The MO solution was adjusted to pH 3 using 1 M of HCl and 1 M of NaOH prior to reaction initiation. The reaction was activated by hydrogen peroxide (H_2O_2, 12 mM) and stirred 300 rpm at room temperature. The aqueous samples were withdrawn every 15 minutes interval and filtered using 0.2 µm syringe filters. The filtrate samples were immediately analyzed using UV-Vis spectrophotometer (Perkin Elmer, Lamda 25) at the maximum absorbance peak of MO; λ_{max} = 464 nm. Similar procedures were carried out using the pristine iron oxides and MKSF as the basis of references for the pristine catalytic properties.

3. Results and Discussion

The physico-chemical properties Fe-MKSF catalyst was determined through the collective findings of nitrogen sorption, XRD, TG-DTG analysis. The pristine MKSF and iron oxide catalyst were used as the basis of reference in understanding the changes in Fe-MKSF once the iron species were successfully immobilized onto and/or MKSF clay matrix. Fig. 1 displays the nitrogen adsorption-desorption isotherm of the MKSF clay, Fe-MKSF and iron oxide. MKSF exhibited a type III isotherms with H3 hysteresis at relative pressure ranging from 0.48 to 0.99. The type III isotherm represents the relatively weak adsorbent-adsorbate interactions, where the adsorbed molecules are clustered around the most favorable sites on the surface of nonporous material [34]. The H3 hysteresis loop reveals the non-rigid aggregates of plate-like material consisting of slit-shaped pores that typically associated with clay type materials [35]. This observation is in agreement with the reported double faced lamellae structures of MKSF clay as reported by Shahidi et al. [1]. The iron oxides also exhibited type III isotherms but a notable change in hysteresis was observed. The hysteresis fit to the H1 type at the relative pressure ranging from 0.8 to 0.98, which can be attributed to the network of mesopores and interparticle space.

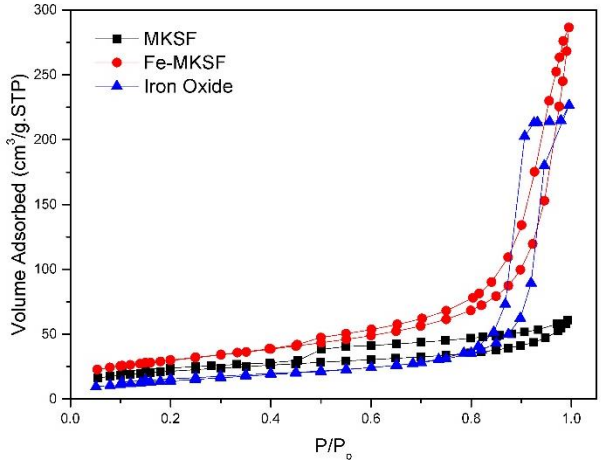

Fig. 1: Nitrogen adsorption-desorption isotherms of MKSF, Fe-MKSF and iron oxide catalyst

Similar isotherm (type III) with a slight shift in H3 hysteresis at the relative pressure from 0.45 to 0.99 was observed for Fe-MKSF catalyst. Interestingly, the Fe-MKSF catalyst displayed a significant increment for the total quantity of the volume adsorbed which found to be approximately 6 time higher (~285 cm^3/g STP at relative pressure of 0.99) than the pristine MKSF clay (~51 cm^3/g STP). In addition, the slight shift to the lower relative pressure with vicissitudes in the volume adsorbed of hysteresis loop signified the mesoporous structure of Fe-MKSF catalyst which possessed a certain degree of variances during the adsorption and desorption processes. Such changes indicated plausible intercalation of iron oxide in between the interlamellar spaces of MKSF clay during the synthesis process. Relatively,

similar observations were also reported in the previous works [36-38] once the active catalysts being successfully immobilized onto different types of the catalyst support.

The structural properties of the catalyst can be further understood by pore size distribution as shown in Fig. 2. The pore size distributions of pristine MKSF were centred at 10, 15 and 65 nm. Once the iron oxides being immobilized within the MKSF structure, clear enlargement of pore size distribution was visible. Interestingly, the pore size distribution of Fe-MKSF catalyst shown pore size ranging from 8 nm to 50 nm with some presence of macropores ranging from 50-70 nm that can be associated with the beneficial intercalation of iron oxides particles between the interlamellar spaces of MKSF clay.

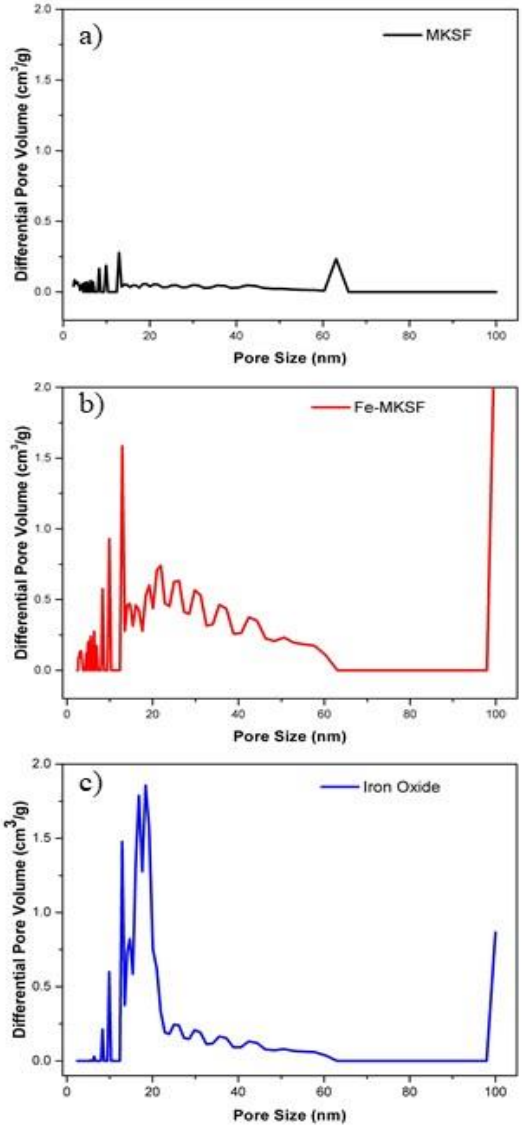

Fig. 2: Pore size distribution of a) MKSF, b) Fe-MKSF and c) iron oxide catalyst.

Fig. 3 shows the surface area and pore volume for the MKSF, Fe-MKSF and iron oxides. A significant increment in surface area was observed by order of magnitude from 52.2 m^2/g (iron oxide) to 105.8 m^2/g (Fe-MKSF) once the iron oxide particles being immobilized within the structure of MKSF clay. In fact, the pore volume of Fe-MKSF catalyst was found to increase by 26% and 388% than the pristine iron oxides and MKSF clay, respectively. Such vicissitudes in surface area and pore volume are favorable in having the high accessibility of reactants towards the active sites ($\equiv Fe^{2+}/\equiv Fe^{3+}$), which are able to diminish limitations in mass transfer during the reaction as reported elsewhere [14].

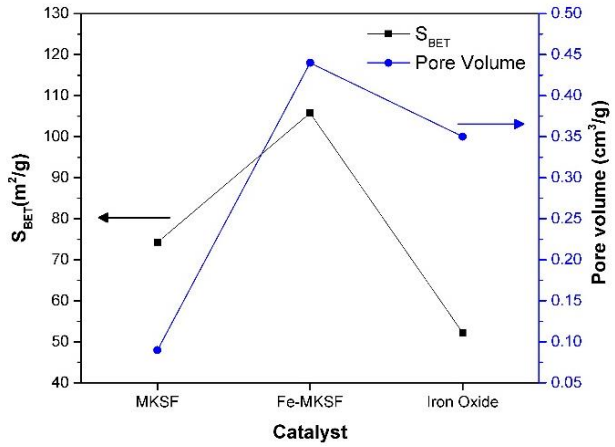

Fig. 3: BET surface area and pore volume of MKSF, Fe-MKSF and iron oxide catalyst

The XRD patterns of pristine MKSF, Fe-MKSF and iron oxides catalyst are displayed in Fig. 4. The iron oxides catalyst exhibited with the crystal structure of hematite (α-Fe_2O_3), indexed to PDF-01-087-1165 with diffraction peaks at 2θ = 25.12°, 33.08° and 35.63°.These diffraction peaks were assigned by (012), (104), and (110) crystal planes, respectively. The main peak of hematite with the highest intensity was clearly observed for iron oxide at 2θ value of 25.12°. Similar diffraction peak at 2θ value of approximately 25.12° was also visible in Fe-MKSF, but at the lower peak intensity. The presence of MKSF clay as catalyst support did not affect the phase transformation of iron oxides phase which was found to be remained in the rhombohedral hematite phase. Uniquely, this finding was contradict with the previous work of Katikaneani et al. [39], whom reported that the iron oxide experienced the phase transformation from hematite to maghemite phase in the presence of organic support i.e. polyethyelene glycol. These interesting findings warrant the unique characteristic of MKSF that implied with inert influence toward the transformation of iron oxides phase during the synthesis process at the specified operating temperature.

The thermogravimetric analysis was carried out using uncalcined samples. Fig. 5 presents the thermogravimetric-differential thermogravimetric (TG-DTG) curves of the MKSF, Fe-MKSF and iron oxides respectively. MKSF showed a single mass loss pattern only at temperature range of 50°C -150°C. The percentage of mass loss at this temperature range was approximately 13.3%. This mass loss may be ascribed to the nature-rich metallic cations in montmorillonite and the high acidity value that resulted from the presence of Bronsted and Lewis acids sites [40]. There was no other thermal decomposition activity for MKSF because the metallic cation in montmorillonite was very stable and was not affected by the temperature change.

Iron oxide and Fe-MKSF catalysts showed two visible mass loss patterns in the TG-DTG thermograms. The first pattern was observed within the range from 50°C to 120°C and the second pattern was at the range from 200°C to 270°C. The initial mass loss at a temperature range from 50°C to 120°C was assigned to the removal of physisorbed water in the catalyst due to the elimination of interlayer water molecules bound to the resultant catalyst. The later thermal decomposition within 200°C-270°C was attributed to the phase change or transformation process of iron oxides from the magnetite into the hematite phase. Such observation was in line with the findings of Farbod et al. [41] and Bhavani et al. [42], whom reported that the iron oxide is thermodynamically transformed to hematite phase at temperature above 300°C. A shift of a distinct peak of DTG curve during the phase transformation was observed between the iron oxide (~250°C) and Fe-MKSF (~265°C).

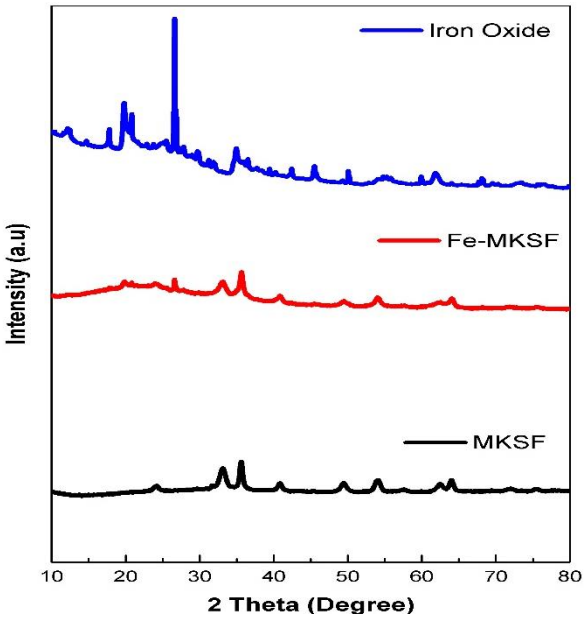

Fig. 4: XRD patterns for MKSF, Fe-MKSF and iron oxide catalyst

The profiling of oxidative degradation of MO using the Fe-MKSF, iron oxide and MKSF catalysts are shown in Fig. 6. The iron oxide showed favourable discoloration for the first 30 minutes of reaction prior to the complete deactivation afterwards. Interestingly, the catalytic deactivation of iron oxide was circumvented once the iron were being immobilized within the MKSF matrix. The Fe-MKSF catalyst exhibited stable catalytic activity throughout the reaction which able to remove up to 85% of MO. Such exceptional performance of Fe-MKSF was plausible due to synergistic interaction of MKSF and the iron oxide during catalysis. These results were in agreement with previous researchers that observed the similar interaction between the iron oxide and kaolin clay [43]. The presence of MKSF clay as catalyst support in Fe-MKSF plays vital role in modulating the physico-chemical properties, which directly corresponded to the resultant catalytic activity of Fe-MKSF. Such enhancement in catalytic activity can be well supported by the unique characteristics of MKSF clay that was known to be metal-(especially iron)-rich materials [44] which able to concurrently decompose oxidant (H_2O_2) in producing more reactive radicals during the heterogeneous Fenton-like catalysis.

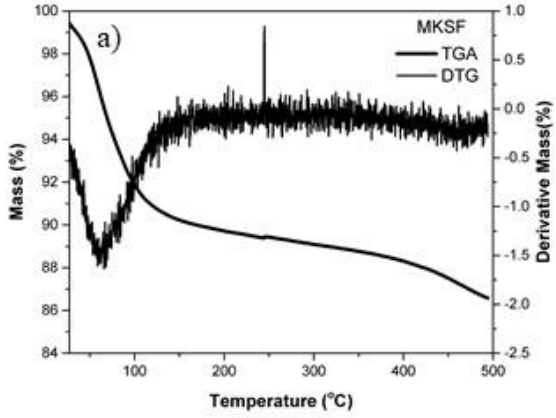

(a)

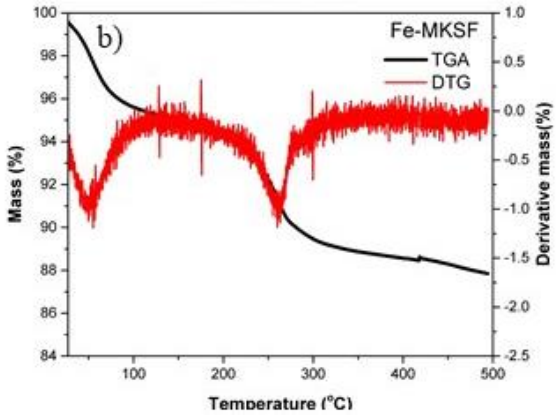

(b)

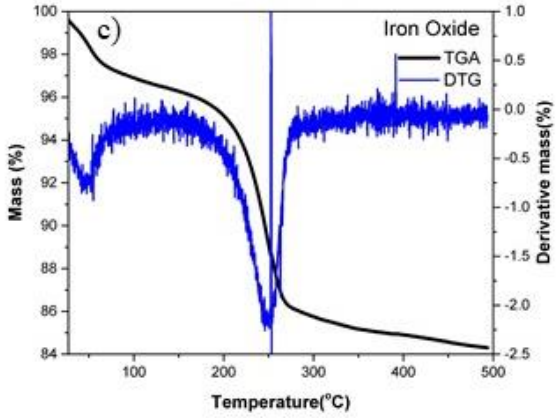

(c)

Fig. 5: TG-DTG thermograms for (a) MKSF, (b) Fe-MKSF and (c) iron oxide

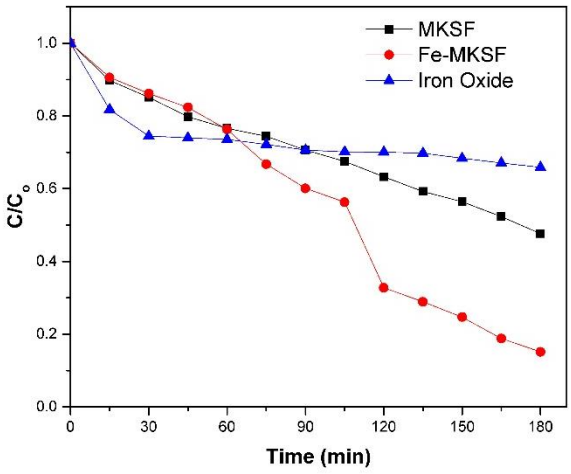

Fig. 6: MO discoloration by heterogeneous Fenton-like reaction (Condition: pH 3, 0.2 g/L catalyst, 35 mg/L, and 12 mM H_2O_2)

4. Conclusion

In-depth understanding on the physico-chemical properties towards modulating the catalytic activity for the resultant Fe-MKSF were obtained through the collective findings of nitrogen sorption, XRD and TGA analysis. Interestingly, the presence of MKSF plays a crucial role in modulating the physico-chemical and catalytic properties of Fe-MKSF catalyst. Based on the findings, the Fe-MKSF showed a significant increment in surface area (105.8 m^2/g) and pore volume (0.45 cm^3/g) once the iron oxide particles being immobilized onto and/ or within the structure

of MKSF clay. Such changes in both features are favourable in providing high accessibility of reactants towards the active sites ($\equiv Fe^{2+}/\equiv Fe^{3+}$) of the resultant catalyst, which are able to diminish limitations in mass transfer during heterogeneous Fenton-like catalysis. Interestingly, the presence of MKSF clay as catalyst support did not affect the phase transformation of iron oxides phase which was found to be remained in the rhombohedral hematite phase that in tandem with the TGA findings. In conclusions, these traits proved to be essential for the enhancement of Fe-MKSF's catalytic activity (85% MO removal) due to the plausible synergistic interactions between the MKSF and iron oxide during the heterogeneous Fenton-like catalysis.

Acknowledgement

The authors gratefully acknowledged the Ministry of Higher Education Malaysia (MOHE) and Universiti Teknologi MARA (UiTM) for financial support under the Fundamental Research Grant Scheme (600-IRMI/FRGS 5/3 (110/2016)). J.C. Diniz da Costa thanks the support from the ARC via the Future Fellowship Program (FT130100405).

References

[1] Shahidi D, Roy R, & Azzouz A (2015), Advances in catalytic oxidation of organic pollutants - Prospects for thorough mineralization by natural clay catalysts. *Appl. Catal. B Environ*. 174–175, 277–292.

[2] Tantak NP & Chaudhari S (2006), Degradation of azo dyes by sequential Fenton's oxidation and aerobic biological treatment. *J. Hazard. Mater*. 136, 698–705.

[3] Chen Q, Wu P, Dang Z, Zhu N, Li P, Wu J. & Wang X (2010), Iron pillared vermiculite as a heterogeneous photo-Fenton catalyst for photocatalytic degradation of azo dye reactive brilliant orange X-GN. *Sep. Purif. Technol.* 71, 315–323.

[4] Yaseen DA & Scholz M (2018), Treatment of synthetic textile wastewater containing dye mixtures with microcosms, *Environ. Sci. Pollut. Res*. 25, 1980–1997.

[5] Karthikeyan S, Titus A, Gnanamani A, Mandal AB & Sekaran G (2011), Treatment of textile wastewater by homogeneous and heterogeneous Fenton oxidation processes. *Desalination* 281, 438–445.

[6] Yeh CKJ, Hsu CY, Chiu CH & Huang KL (2008), Reaction efficiencies and rate constants for the goethite-catalyzed Fenton-like reaction of NAPL-form aromatic hydrocarbons and chloroethylenes. *J. Hazard. Mater*. 151, 562–569.

[7] Chen H, Motuzas J, Martens W & Diniz da Cost JC (2018), Degradation of orange II dye under dark ambient conditions by MeSrCuO (Me = Mg and Ce) metal oxides. *Sep. Purif. Technol*. 205, 293-301.

[8] Aznárez A, Delaigle R, Eloy P, Gaigneaux EM, Korili S,& Gil A (2015), Catalysts based on pillared clays for the oxidation of chlorobenzene. *Catal. Today* 246, 15–27.

[9] Soon AN & Hameed BH (2011), Heterogeneous catalytic treatment of synthetic dyes in aqueous media using Fenton and photo-assisted Fenton process. *Desalination* 269, 1–16.

[10] Ersöz G (2014), Environmental Fenton-like oxidation of Reactive Black 5 using rice husk ash based catalyst. *Applied Catal. B Environ*. 147, 353–358.

[11] Wang Y, Sun Y, Li W, Tian W & Irini A (2015), High performance of nanoscaled Fe_2O_3 catalyzing UV-Fenton under neutral condition with a low stoichiometry of H_2O_2 : Kinetic study and mechanism. *Chem. Eng. J*. 267, 1–8.

[12] Li Y, Lu Y & Zhu X (2006), Photo-Fenton discoloration of the azo dye X-3B over pillared bentonites containing iron. *J. Hazard. Mater*. 132, 196–201.

[13] Sum OSN, Feng J, Hub X & Yue PL (2005), Photo-assisted fenton mineralization of an azo-dye acid black 1 using a modified laponite clay-based Fe nanocomposite as a heterogeneous catalyst. *Topic Catal*. 33, 233–242.

[14] Zubir NA, Yacou C, Motuzas J, Zhang X, &. Diniz da Costa JC (2014), Structural and functional investigation of graphene oxide-Fe_3O_4 nanocomposites for the heterogeneous Fenton-like reaction. *Sci. Rep*. 4, 4594.

[15] Avetta P, Pensato A, Minella M, Malandrino, Maurino V, Minero C, Hanna K & Vione D (2015), Activation of persulfate by irradiated magnetite: implications for the degradation of phenol under heterogeneous photo-Fenton-like conditions. *Environ. Sci. Technol.* 49, 1043–1050.

[16] Muthuvel I, Krishnakumar B & Swaminathan M (2012), Solar active fire clay based hetero-Fenton catalyst over a wide pH range for degradation of Acid Violet 7. *J. Environ. Sci*. 24, 529–535.

[17] Pérez A, Montes M, Molina R & Moreno S (2014), Modified clays as catalysts for the catalytic oxidation of ethanol. *Appl. Clay Sci.* 95, 18–24.

[18] Hassan H & Hameed BH (2011), Oxidative decolorization of Acid Red 1 solutions by Fe-zeolite Y type catalyst. *Desalination* 276, 45–52.

[19] Queirós S, Morais V, Rodrigues CSD, Maldonado-Hódar FJ &. Madeira LM (2015), Heterogeneous Fenton's oxidation using Fe/ZSM-5 as catalyst in a continuous stirred tank reactor. *Sep. Purif. Technol.* 141, 235–245.

[20] Yaman C & Gündüz G (2015), A parametric study on the decolorization and mineralization of C.I. Reactive Red 141 in water by heterogeneous Fenton-like oxidation over FeZSM-5 zeolite. *J. Environ. Heal. Sci. Eng*. 13, 1–12.

[21] Shukla P, Wang S, Sun H, Ang HM & Tadé M (2010), Adsorption and heterogeneous advanced oxidation of phenolic contaminants using Fe loaded mesoporous SBA- 15 and H_2O_2. *Chem. Eng. J*. 164, 255–260.

[22] Xiang L, Royer S, Zhang H, Tatibouët J, Barrault J & Valange S (2009), Properties of iron-based mesoporous silica for the CWPO of phenol : A comparison between impregnation and co-condensation routes. *J. Hazard. Mater*. 172, 1175–1184.

[23] Zubir NA, Yacou C, Motuzas J, Zhang X, Zhao XS & Diniz da Costa JC (2015), The sacrificial role of graphene oxide in stabilising Fenton-like catalyst GO–Fe_3O_4. *Chem. Commun* 51, 9291-9293.

[24] Zubir NA, Yacou C, Zhang X & Diniz da Costa JC (2014), Optimisation of graphene oxide–iron oxide nanocomposite in heterogeneous Fenton-like oxidation of acid orange 7. *J. Environ. Chem. Eng.* 2, 1881–1888.

[25] Duarte F, Maldonadohódar FJ & Madeira LM (2012), nfluence of the particle size of activated carbons on their performance as Fe supports for developing fenton-like catalysts. *Ind. Eng. Chem. Re*s. 51, 92188–9226.

[26] Duarte FM, Maldonadohódar FJ & Madeira LM (2013), Influence of the iron precursor in the preparation of heterogeneous Fe / activated carbon Fenton-like catalysts. *Applied Catal. A, Gen*. 458, 39–47.

[27] Ramirez JH, Maldonadohódar FJ, Pérez-Cadenas F, Moreno-Castilla C, Costa C &Madeira LM (2007), Azo-dye orange II degradation by heterogeneous Fenton-like reaction using carbon-Fe catalysts. *Appl. Catal. B Environ*. 75, 312–323.

[28] Ellias N & Sugunan S (2014), Wet peroxide oxidation of phenol over cerium impregnated aluminium and iron- aluminium pillared clays. *IOSR J. Appl. Chem*. 7, 80–85.

[29] Liu Z, Ma H, Liu J, Xing L, Cheng L, Yang J, Mao B & Zhang Q (2018), A low-cost clay-based heterogeneous Fenton-like catalyst: Activation, efficiency enhancement, and mechanism study. *Asia-Pacific J. Chem. Eng.* 13, 1–13.

[30] Hassan H & Hameed BH (2011), Fenton-like oxidation of Acid Red 1 solution using heterogenous catalyst based on Ball clay. *Int. J. Environ. Sci. Dev.* 2, 218–222.

[31] Tiya-Djowe A, Ruth N, Kamgang-Youbi G, Acayanka E, Laminsi S & Gaigneaux EM (2018), FeOx-kaolinite catalysts prepared via a plasma-assisted hydrolytic precipitation approach for Fenton-like reaction. *Microporous Mesoporous Mater*. 255, 48–155.

[32] Garrido-Ramírez EG, Theng BKG & Mora ML (2010), Clays and oxide minerals as catalysts and nanocatalysts in Fenton-like reactions - A review. *Appl. Clay Sci.* 47, 182–192.

[33] Feng J, Hu X, Yue PL, Zhu HY & Lu GQ (2003), Degradation of azo-dye orange II by a photoassisted Fenton reaction using a novel composite of iron oxide and silicate nanoparticles as a catalyst. *Ind. Eng. Chem. Res*. 42, 2058–2066.

[34] Thommes M, Kaneko K, Neimark AV, Oliver JP, Rodriguez-Reinoso F, Rouquerol J & Sing KSW (2015), Physisorption of gases, with special reference to the evaluation of surface area and pore size distribution (IUPAC Technical Report). *Pure Appl. Chem.* 87, 1051–1069.

[35] Li H, Li Y, Xiang L, Huang Q, Qiu J, Zhang H, Siviah MV, Baron F, Barrault J, Petit S & Valange S (2015), Heterogeneous photo-Fenton decolorization of Orange II over Al-pillared Fe-smectite: Response surface approach, degradation pathway, and toxicity evaluation. *J. Hazard. Mater.* 287, 32–41.

[36] Zhao Z, Dai H, Deng J, Liu Y, Wang Y, Li X, Bai G, Gao B & Au CT (2013). Porous FeOx/BiVO4-S0.08: Highly efficient photocatalysts for the degradation of methylene blue under visible-light illumination. *J. Environ. Sci. (China)* 25, 2138–2149.

[37] Bagheri S, Julkapli NM & Hamid SBA (2014), Titanium dioxide as a catalyst support in heterogeneous catalysis. *Scientific World J*., ID 727496, 1–21.

[38] Pan J, Wang C, Guo S, Li J & Yang Z (2008), Cu supported over Al-pillared interlayer clays catalysts for direct hydroxylation of benzene to phenol. *Catal. Commun*. 9, 176–181.

[39] Katikaneani P, Vaddepally AK, Tippana NR, Banavath R & Kommu S (2016), Phase transformation of iron oxide nanoparticles from hematite to maghemite in presence of polyethylene glycol : application as corrosion resistant nanoparticle paints. *J. Nanosci*., ID 1328463, 1–6.

[40] Bieseki L, Treichel H, Araujo AS, Berenice S & Pergher C (2013), Porous materials obtained by acid treatment processing followed by pillaring of montmorillonite clays. *Appl. Clay Sci*. 85, 46–52.

[41] Farbod M, Movahed A & Kazeminezhad I (2012), An investigation of structural phase transformation of monosize γ-Fe_2O_3 nanoparticles fabricated by arc discharge method. *Mater. Lett.*, 89, 140–142.

[42] Bhavani P. Reddy NR, Reddy IVS & Sakar M (2017), Manipulation over phase transformation in iron oxide nanoparticles via calcination temperature and their effect on magnetic and dielectric properties. *IEEE Trans. Magn*. 53, 1–5,.

[43] Daud NK & Hameed BH (2011), "Acid Red 1 dye decolorization by heterogeneous Fenton-like reaction using Fe/kaolin catalyst. *Desalination* 69, 291–293.

[44] Chen L, Deng C, Wu F & Deng N (2011), Decolorization of the azo dye Orange II in a montmorillonite/H_2O_2 system. *Desalination* 281, 306–311.